IEEE Access
Multidisciplinary | Rapid Review | Open Access Journal

Received 13 November 2023, accepted 25 November 2023, date of publication 28 November 2023,
date of current version 5 December 2023.

Digital Object Identifier 10.1109/ACCESS.2023.3337373

RESEARCH ARTICLE

Korean Renewables Management System: Copulas Model-Based Adaptive Droop Control Strategy for Energy Storage Systems

SUNGYOON SONG[1], (Member, IEEE), SUNGWOO KANG[2], (Graduate Student Member, IEEE), SANGHO LEE[1], (Member, IEEE), AND CHANG KI KIM[3], (Member, IEEE)

[1]Department of Advanced Power Grid Research, Korea Electrotechnology Research Institute, Uiwang-si 16029, South Korea
[2]School of Electrical Engineering, Korea University, Seoul 02841, South Korea
[3]Renewable Energy Big Data Laboratory, Korea Institute of Energy Research, Daejeon 34129, South Korea

Corresponding author: Chang Ki Kim (ckkim@kier.re.kr)

This work was supported in part by the Korea Institute of Energy Technology Evaluation and Planning Grant funded by the Korean Government [Ministry of Trade, Industry and Energy (MOTIE)] under Grant 2019371010006B, and in part by the National Research Foundation of Korea (NRF) Grant funded by the Korean Government [Ministry of Science and ICT (MSIT)] under Grant RS-2023-00218377.

ABSTRACT To achieve the goal of carbon neutrality, increasing the contribution of renewable energy sources (RESs) such as solar and wind to power grids is necessary. However, existing energy management systems are not well-equipped to handle the inherent volatility of RESs, and previous attempts to develop new management systems have mostly been limited to small scales such as microgrids and buildings. The Korea Electrotechnology Research Institute and Korea Institute of Energy Research jointly developed a renewables management system (RMS) for large-scale grids that comprises four parts: a 12-h-ahead solar irradiance forecast model; look-ahead horizon stability assessment; generation o f future RES penetration scenarios by a generative adversarial networks model; and confidence level-based adaptive droop control strategy for energy storage systems. In particular, the adaptive droop control obtains the joint probability distribution at each substation based on copula theory, and the droop gain changes with the confidence level. Simulations were performed to demonstrate the effectiveness of the proposed RMS at managing large-scale grids with high RES penetration.

INDEX TERMS Renewable management system, forecast, copula theory, adaptive droop control, energy storage system.

I. INTRODUCTION

The rapid development of renewable energy sources (RESs) such as solar and wind power is expected to play an important role in achieving the goal of carbon neutrality and stimulating the global economy [1]. South Korea is aiming to achieve carbon neutrality before 2050, and many domestic scholars have focused on contributing to this goal [2]. Two solutions have been proposed to achieve carbon neutrality: increasing RES utilization to 400 GW to replace fossil fuels and increasing energy efficiency by integrating RESs and energy storage systems (ESS). South Korea has an ambitious goal to achieve 70% RES generation ratio by 2050, and to phase out fossil fuel power generation. Due to geographical limitations, the solar installation rate is overwhelmingly higher than that of wind energy, necessitating a greater capacity of solar. However, the intermittency of solar power requires revolutionary changes in grid operation and planning [3]. In 2050, ±4GW variation can occur when there is a 1% of forecast error in peak level. Accordingly, some of the most pressing issues are the development of practical and precise forecast techniques and look-ahead horizon stability assessment. Thus, some researchers have argued that a separate renewables management system (RMS) should be developed

The associate editor coordinating the review of this manuscript and approving it for publication was Jahangir Hossain.

to compensate existing centralized energy management systems. Therefore, the proposed RMS system aims to focus on the enhancement of RESs forecasting technologies and the control of ESS at the substation level. Some attempts have already been made to develop various RMS architectures, as shown in Table 1.

TABLE 1. Previous studies on key functions in RMS.

RES forecasting techniques	Real-time dispatch of generators	Look-ahead stability assessment	Control strategy of ESS
[4-6]	[7-11]	[21-23]	[28-29]

For instance, Mohandes et al. [4] used the multiplicative weight update method with deep learning to improve forecasting. In addition to this, novel deep learning techniques for forecasting the RES supply have been introduced nowadays [5], [6]. However, those techniques suffer in accuracy when frequent curtailment orders occur. Large-scale grids with high RES penetration have too many possible curtailment orders for a given time step. Wrong data can generate inaccurate forecasts, and considering all exceptions is impossible. In addition, mitigating the variability of RESs is generally limited to maximum power point tracking. To address this issue, we propose the lattice-based satellite imaging is used for practical forecasting of RESs. And, many studies have also been conducted on power dispatch in response to changes in RESs generation, and this technology is playing a key role in RMS systems. For example, Solanki et al. [7] incorporated various optimization algorithms for hourly dispatch of a microgrid. Yang et al. [8] optimized the power flow for economic efficiency to realize practical real-time control of distributed generators. And, Cui et al. [9] considered both the equivalent CO_2 emissions and operating costs for dispatch of a microgrid. Barchi et al. [10] and Dinh et al. [11] both proposed rule-based control schemes for distributed generators in buildings and homes. As mentioned earlier, these studies mostly considered RMSs for small-scale power grids, such as microgrids, buildings, and homes.

Unfortunately, RMS systems have been predominantly developed and researched for distributed generators in small-scale network, rather than for large-scale power systems. Note that, grid operators cannot combine multiple RMS architectures that have their own management algorithms. Furthermore, grid operators cannot regulate the power of non-dispatchable RESs. In South Korea, meticulous preparations are ongoing for the formulation of a virtual power plant and bidding market for RESs. However, RESs are not obligated to satisfy grid regulations extracted from the recent IEEE standards IEEE 1547 or IEEE 2800, and there are inherent update issues with coordinating control schemes for existing distributed generators. An effective way to address RES variability in South Korea is to predict the power supply at each substation and eliminate variability in real-time by using ESSs.

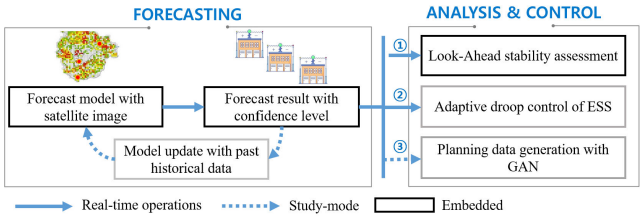

FIGURE 1. Proposed architecture of the RMS.

Therefore, this paper presents an advanced RMS that was jointly developed by the Korea Electrotechnology Research Institute (KERI) and Korea Institute of Energy Research (KIER), as shown in Fig. 1. The Korean RMS uses copula theory to derive a confidence level based on past and current forecast data. Given the high proportion of solar power in South Korea, integrating forecast accuracy metrics into the system control logic is essential. Thus, the Korean RMS incorporates both look-ahead horizon stability assessment and an adaptive droop control scheme for the ESS. Several studies have demonstrated that adaptive droop control of the ESS based on copula theory is an effective approach [12], [13]. Rather than a monitoring system, the Korean RMS should be considered a control system. Previous studies have not considered a control strategy for the ESS that considers the confidence level of the RESs. Thus, an advanced control strategy is introduced that considers the forecast uncertainty of RESs to minimize curtailment orders and properly manage the state of charge (SOC) of the ESS. For grid planning, the investment costs for future substations and transmissions depend on the RES patterns. Many physical model-based methods have difficulties with handling uncertainties from stochastic changes inherent to some RESs. Using representative values for RESs can leads to inaccurate investments in future grids [14]. Thus, a generative adversarial networks (GAN) model was utilized derive meaningful RES patterns at each substation that are fully utilized for grid planning. The main contributions of the Korean RMS can be summarized as follows:

- Lattice-based satellite imaging is used for precise forecasting of RESs. RESs can be fully observed for each substation without making any changes to the model.
- Grid data are generated, and over 10 types of stability assessments are performed in 5-min intervals. The stability results are organized in an SQL database and are displayed by the RMS.
- The forecast data are used as inputs of the GAN model [15] to obtain future RES penetration scenarios for grid planning.
- An adaptive droop control scheme for ESSs based on copula theory is introduced to minimize curtailment. The control logic depends on the confidence level of the RESs. Any control strategy can be integrated with the RMS.

The rest of the paper is organized as follows. Section II introduces the architecture of the Korean RMS. Section III describes the adaptive droop control of the ESS based on copula theory. Section IV presents simulations used to evaluate the performance of the Korean RMS. Section V concludes the paper.

II. KOREAN RENEWABLES MANAGEMENT SYSTEM

The Korean RMS was installed in KERI, and a data communication structure has been constructed between the email servers of KERI and KIER. The Korean RMS can be divided into four main parts, which are described below.

A. FORECASTING SOLAR IRRADIANCE BASED ON SATELLITE IMAGING

The forecast model of the Korean RMS is focused on forecasting the solar irradiance because solar power makes up a large proportion of RESs in South Korea. The Unified Model–Local Data Assimilation and Prediction System (UM-LDAPS) [16] operated by the Korea Meteorological Administration is employed for the 12-h-ahead solar irradiance forecast. UM-LDAPS is usually initialized four times per day (i.e., 03:00, 09:00, 15:00, and 21:00 Korean Standard Time (KST)), and the forecast horizon is increased by up to 48 h from each initialization. In this study, the 48-h forecast initialized at 03:00 KST each day was utilized. Owing to spin-up time, the modeling output was valid 5 h after the simulation began. Therefore, the time domain was set to 08:00–20:00 KST each day. To reduce the intrinsic bias of UM-LDAPS, the analog ensemble method was used to forecast each grid cell. This method is used to post-process forecast data by utilizing historical analogs to forecast future events or conditions [17], and it is based on the concept that similar patterns in the past tend to be associated with similar outcomes in the future:

$$\|F_t, A_t\| = \sum_{i=1}^{N_v} \frac{w_i}{\sigma_{fi}} \sqrt{\sum_{j=-k}^{k} (F_{i,t-j} - A_{i,t+j})^2}. \quad (1)$$

where F_t is the current deterministic forecast at a future time t, A_t is the analog forecast for the same time and location valid at a past time t', N_v is the number of physical variables, w_i is the weight of each variable, σ_{fi} is the standard deviation of the training time series, and k is the half of the number of additional times computed. Note that t' represents the elapsed time in the concept of window time, so t' denotes the previous time in the time series data. (1) requires at least two physical variables, which in this study were defined as the direct normal irradiance (DNI) and global horizontal irradiance (GHI) and were weighted equally. The final forecast is the average of the analog ensemble members. The number of analogs to be used and the length of the training period can also influence the forecast accuracy.

The analog ensemble method has several steps [18]. First, the forecast and historical variables are defined. To determine GHI, a composite 2-year dataset (2018–2019) from UM-LDAPS was equally divided into historical analog (2018) and verification (2019) datasets. Observation data were retrieved from the University of Arizona Solar Irradiance Based on Satellite–KIER (UASIBS-KIER) model, which estimates the solar irradiance every 10 min for the Korean peninsula by using the GK–2A L1B dataset as shown in Fig. 2a. A collocation process was performed because of the different grid spacings for UM-LDAPS (i.e., 2 km) and UASIBS-KIER (i.e., 500 m). Then, the physical variables of the UM-LDAPS model were selected with their corresponding weights. As noted above, GHI and DNI were used as predictors with equal weightings because they provide analogous data. Finally, the analog ensemble method was performed by computing the distance of every lead from past forecasts issued at the same time. Forecasts were made based on independent searches. The data were then arranged, and the forecast with the smallest distance was selected. The average value of the selected analogs was calculated, which was set as the forecast for the same lead time and location. These steps are important because they eliminate cumulative error and missing forecasts. The analog ensemble method with UM-LDAPS and UASIBS-KIER forecasts the hourly mean solar irradiance, which can be interpolated into the 30-min average solar irradiance by using the clearness index.

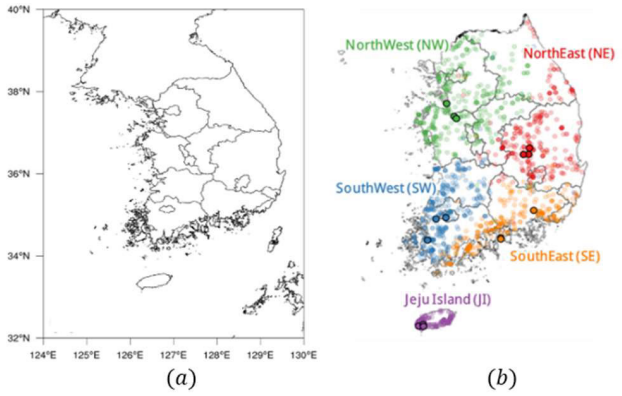

FIGURE 2. (a) Domain for the UASIBS-KIER model; (b) cluster groups.

TABLE 2. Verification results.

	All	NE	SW	NW	JI	SE
nRMSE	6.73	6.84	6.96	6.64	7.28	6.58

Table 2 summarizes the verification results. Considering all grid cells over the Korean peninsula would have been too much for analysis, so cluster analysis was performed to group the forecasts, as shown in Fig. 2b. The nominal root mean square error (nRMSE) was 6.73% on average over the Korean peninsula, and the lowest nRMSE was in the southeast (SE) region. This may be because the SE region receives a higher annual solar irradiance than the rest of South Korea [19]. Finally, the locations of each substation were mapped onto all grid cells over the Korean peninsula. The distance between a RES-based power plant location and

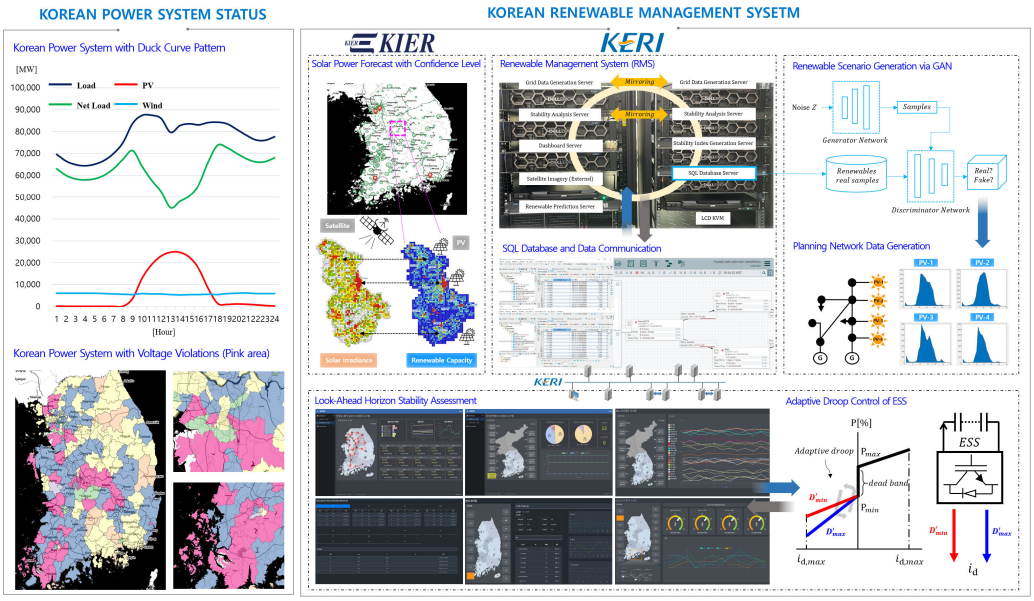

FIGURE 3. Architecture of the proposed Korean RMS for grid operation and planning.

grid cells was formulated by considering the sphere of Earth's surface as a haversine function.

B. LOOK-AHEAD HORIZON STABILITY ASSESSMENT

Recent studies on online power system stability assessment technology predominantly employ deep learning methodologies. However, our system leverages existing commercial software to evaluate the future power system stability. This methodology aligns with conventional approaches seen in previous research [21], [22], [23]. In our study, the stability assessments are conducted based on data acquired from SCADA (Supervisory Control and Data Acquisition) systems, rather than relying on high-resolution measurement devices such as PMUs (Phasor Measurement Units). For the look-ahead horizon stability assessment, multiple static and dynamic parameters are assessed for their stability in real time by using Python and Power System Simulator for Engineering (PSS®E), as detailed in Table 3 and Fig. 3. The current network data (.*raw) and forecast results (.xlsx) for each substation are integrated to obtain the look-ahead horizon stability. The main Python function calls multiple sub-functions simultaneously, which perform designated stability analyses by using the created future network data. To mitigate the calculation time for PSS®E, the results are transferred to a dashboard server in 5-min intervals through the multi-tenant Apache NiFi socket, which is an open-source data communication tool. Inter-area power flow analysis, fault current analysis, contingency analysis, and dynamic analysis calculation times are 0.76, 26.4, 18.09, and 60 seconds, respectively.

C. CONFIDENCE LEVEL BASED ON A COPULA THEORY

For a variable droop gain, the confidence level (i.e., forecast accuracy) of the look-ahead horizon stability assessment

TABLE 3. Look-ahead stability assessment with PSS® E.

Static	• Transmission overloads & bus voltage violations, • System Inertia & total reserve, • Fault currnet & fault capacity & Thevenin impedance, • Contingecny anaysis, • Zonal info (flow, generation, load, capacity, short • circuit ratio), • Weather info (irradation, temperature, precipitation), • RES info (generation, capacity, location, confidence • level, Net-load)
Dynamic	• Freqeuncy stability (rate of change of frequency, • Minimum frequency), • Angle stability (angle spread)

should be calculated. For the Korean RMS, the confidence level (p) is obtained as follows. First, the correlation between variables can be determined by using Pearson's correlation coefficient r_{xy} for the bivariate case [20], as shown in (2).

$$r_{xy} = \frac{\sum_{i=1}^{n} (x_i - \bar{x})(y_i - \bar{y})}{\sqrt{\sum_{i=1}^{n} (x_i - \bar{x})^2} \sqrt{\sum_{i=1}^{n} (y_i - \bar{y})^2}} \tag{2}$$

where $\bar{x}$ and $\bar{y}$ are the average values of each variable. r_{xy} depicts the linear correlation between variables, but it cannot fully represent the interdependency or correlational characteristics between them [21]. Thus, a copula-based approach was used to analyze the interdependency between the historical and current forecast data. The copula is a multivariate cumulative distribution function that can be defined for variables following a uniform distribution. Based on Sklar's theorem, the bivariate case is expressed as follows:

$$H(x, y) = C\left(F_x(x), F_y(y)\right) \tag{3}$$

where H denotes a joint distribution function, and C and F_x denote the copula and cumulative distribution function (CDF), respectively [22]. As noted above, the copula-based approach requires variables to follow a uniform distribution in the range [0, 1]. To analyze the forecast and measured data, variables should be transformed into CDFs, after which the data are transformed into rank parameters with a uniform distribution. Then, the copula-based approach is applicable. Note that a CDF requires a probabilistic density function (PDF). Thus, if the variable follows a certain distribution, a parametric approach can be applied. For example, if the wind speed data are known to follow a Weibull distribution, the PDF can be estimated by finding the parameters that can best represent the given data. However, when information on the distribution is not available, this approach cannot be utilized, and a non-parametric approach should be used instead. Kernel density estimation is a non-parametric approach to estimating the PDF of given data based on the defined kernel function [23], as shown in (4).

$$\hat{f}_h(x) = \frac{1}{n}\sum_{i=1}^{n} K_h(x - x_i), \tag{4}$$

In general, a Gaussian function, Epanechikov function, or uniform function is utilized as the kernel function. These are respectively defined below:

$$K_{h,G}(x;\mu,\sigma) = \frac{1}{\sigma\sqrt{2\pi}} e^{-(x-\mu)^2/(2\sigma^2)}, \tag{5}$$

$$K_{h,EP}(x) = \frac{3}{4}\left(1 - x^2\right)(for\ |x| < 1), \tag{6}$$

$$K_{h,u}(x;a,b) = \frac{1}{b-a}(for\ a\ \le x \le b). \tag{7}$$

Then, the copula-based rank correlation and confidence level p can be computed:

$$\left(U_p^{P_M} - P_F\right)\left(L_p^{P_M} - P_F\right) = 0. \tag{8}$$

where P_F is the forecast data, P_M is the measured data, and U_p and L_p are the upper and lower bounds, respectively, of the confidence interval. As shown in Fig. 4, the confidence level analysis is used to obtain the distribution of forecast data when historical data are given. The confidence level p derived from the two kinds of data is then utilized for adaptive droop control of the ESS at each substation.

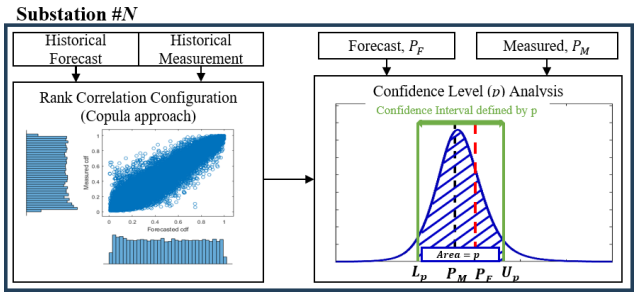

FIGURE 4. Copula-based confidence level analysis for substation N.

D. GENERATING RES PENETRATION SCENARIOS FOR GRID PLANNING

Once the RMS updates the forecast data, future RES penetration scenarios can be created by using a GAN model [14], as shown in Fig. 3. The Korean RMS implements an open-source GAN model [24] in Python. Grid planning requires utilizing past historical data to capture the stochastic characteristics of RESs. Using constant values in a model-based approach can lead to incorrect results. Moreover, assuming numerous scenarios considering the uncertainty of RESs is time-consuming and inefficient. To overcome these issues, the GAN model is used to generate RES penetration scenarios and capture stochastic data. This approach overcomes the difficulties associated with the lack of perfect knowledge of future PDFs. The generated scenarios are then utilized for grid planning.

III. COPULA-BASED ADAPTIVE DROOP CONTROL OF ESS

An adaptive droop control algorithm is used for better ramp-rate control and SOC management of the ESS. As noted earlier, the Korean RMS is considered a control system rather than a monitoring system, so a practical control strategy was developed for large-scale ESSs that are installed at the upper level of substations.

A. VOLTAGE SOURCE INTERFACE OF THE ESS MODEL

An ESS comprises battery cells grouped into modules, which are all housed within a protective shell. These modules are linked in series and in parallel to form a battery string [25]. The ESS includes a voltage source converter (VSC), which enables four-quadrant control. In other words, the real current can be directed to either charging or discharging operations while the reactive current can independently either provide or absorb reactive power. The ESS also depends on the SOC, which represents the available battery energy as a percentage of its total capacity. In this study, the ESS was modeled by combining the plant, electrical, and converter models provided by the WECC.

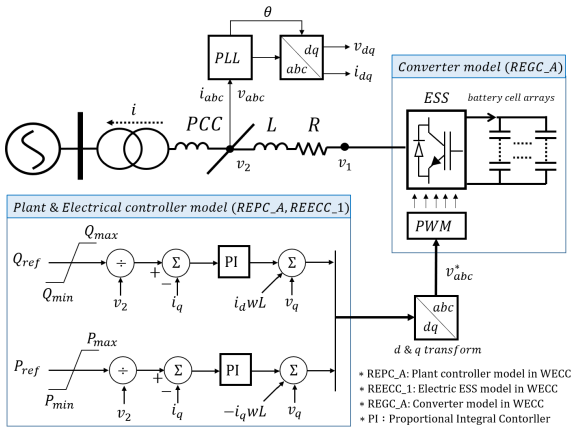

FIGURE 5. ESS control structure with the WECC models.

Fig. 5 shows a typical vector control structure of the ESS. The modeling approach is similar to that used by several

previous studies [26], [27]. The ac system connected to the VSC is modeled in a synchronously rotating reference $d-q$ frame, and the q-axis is locked with the ac voltage to ensure decoupled control. The dynamics on the ac side of the VSC in the $d-q$ frame can be expressed as follows:

$$\begin{bmatrix} v_1^d \\ v_1^q \end{bmatrix} - \begin{bmatrix} v_2^d \\ v_2^q \end{bmatrix} = R\begin{bmatrix} i_1^d \\ i_1^q \end{bmatrix} + L\frac{d}{dt}\begin{bmatrix} i_1^d \\ i_1^q \end{bmatrix} + \begin{bmatrix} -\omega L i_1^q \\ \omega L i_1^d \end{bmatrix}, \quad (9)$$

$$\begin{bmatrix} v_1^d \\ v_1^q \end{bmatrix} - \begin{bmatrix} v_2^d \\ v_2^q \end{bmatrix} = R\begin{bmatrix} i_d \\ i_q \end{bmatrix} + L\frac{d}{dt}\begin{bmatrix} i_d \\ i_q \end{bmatrix} - \begin{bmatrix} -\omega L i_q \\ \omega L i_d \end{bmatrix}. \quad (10)$$

where v_2 is the voltage at the point of common coupling (PCC) and v_1 is the voltage at the VSC. R and L are the resistance and inductance, respectively, while i is the current flowing to the ac system. ω is the angular frequency of the ac voltage at the PCC. The reference voltage generated by the inner current control loop is transformed back into the *abc* frame and pulse with modulation (PWM) to produce the desired converter three-phase voltage. The voltage reference sent to the PWM is represented as follows:

$$\begin{bmatrix} \Delta v_2^d \\ \Delta v_2^q \end{bmatrix} = -\begin{bmatrix} A_d(s) \\ A_q(s) \end{bmatrix}\begin{bmatrix} \Delta i_{d,ref} - \Delta i_d \\ \Delta i_{q,ref} - \Delta i_q \end{bmatrix} + \omega L\begin{bmatrix} -\Delta i_q \\ \Delta i_d \end{bmatrix} + \begin{bmatrix} v_1^d \\ v_1^q \end{bmatrix}, \quad (11)$$

where $A_d(s)$ *and* $A_q(s) = \frac{k_p s + k_i}{s}$. $A_d(s)$ and $A_q(s)$ are proportional–integral controllers, and the q-axis current of the $d--q$ frame is aligned with the ac system phasor based on a phased-locked loop (PLL), i.e., $v_q = 0$. Thus, active, reactive and droop control are all achieved by using $P = 3/2\,(v_d i_d)$ and $Q = -3/2(v_d i_q)$.

B. DESIGN OF ADAPTIVE DROOP CONTROL

To mitigate the variability inherent in RESs, ramp-rate control is frequently implemented with ESSs [28], [29]. The power variation can be represented in (12) and the proposed adaptive droop control strategy is both intuitive and simplistic:

$$\Delta P = \frac{P(t) - P(t - \Delta t)}{P_{nor}}, \quad (12)$$

where ΔP is defined as the difference between two consecutive samples of power normalized to the power P_{nor}. For a standard ramp-rate $R_s(\%)$, P_{ref} for the active power reference of ESS can be calculated as follows:

$$P_{ref} = \begin{cases} \Delta P - R_l, & if\ \Delta P/t_s > R_l, \\ \Delta P + R_l, & if\ \Delta P/t_s < -R_l, \\ 0, & if\ -R_l \le \Delta P/t_s \le R_l. \end{cases} \quad (13)$$

where t_s is the sampling period and R_l is the ramp-rate constraint at the PCC that can be calculated by $(R_s \times P_{nor})/t_s$. At high ramp rates, a constraint is necessary. Considering stable range of SOC, the output of the d-axis current (i_d) injected into the grid should be set as follows:

1) If $SOC(t) > SOC_{max}$, then i_{dmin} is updated to 0.
2) If $SOC_{min} > SOC(t)$, then i_{dmax} is changed to 0.

i_{dmax} and i_{dmin} are the maximum and minimum active current limits, respectively. By forcing these limits to zero when the SOC hits its limits, the ESS is shut down so that it cannot further charge or discharge once at SOC_{max} or SOC_{min}, respectively.

The proposed adaptive droop control strategy is to design the droop gain of P_{ref} in the outer controller. A variable droop is introduced to adjust the rapid charge or discharge at the ESS. However, frequent changes in the droop gain are not desirable for converter stability and SOC. Thus, three droop gains were applied, as shown in Fig. 6: $D_{i,0}, D_{i,min}, D_{i,max}$. The variation in the confidence level is measured after the solar irradiance forecast in 30-min intervals. For M substations, the ith ESS uses the proposed adaptive droop control strategy, and the ESS of each substation has its own confidence level. At any time, the weighted average method can be used to recalculate the confidence level to accommodate additional RESs. For example, if there are two RESs with 95% of 20 MVA and 85% of 10 MVA at one substation, the confidence level can be calculated by $(95\times20 + 85\times10)/(20 + 10) = 91.6\%$. This implies a change in RES capacity at the ith ESS, and the modified confidence level changes the droop gain.

If the power variability ΔP at substation is greater than R_l, then the ith ESS recognizes the need for ramp-rate control with the variable droop gain. This can be achieved by the binary control signal as shown in (14).

$$S = \begin{cases} 0, & if\ \Delta P(t) > R_l, \\ 1, & if\ \Delta P(t) \le R_l, \end{cases} \quad (14)$$

If there is sudden increase in RES power, then ΔP exceeds R_l, and the binary signal S is switched to 0. If ΔP is regulated to within the stable range, then $S = 1$ to return to the original control. After the confidence level p is obtained at each substation, the droop value for the ith ESS is adaptively changed as follows:

$$D_i' = \begin{cases} D_{i,0}, & if\ 0.3 \ge p \ge 0.8 \\ D_{i,min}, & if\ p > 0.8 \\ D_{i,max}, & if\ p < 0.3 \end{cases} \quad (15)$$

A high droop gain is chosen when p is small because this implies high confidence in the forecast accuracy for a given time. Thus, a relatively fast current response flows into the substation to regulate ΔP. In contrast, a relatively slow current response is injected into the substation for SOC management when p is large because the forecast accuracy may be compromised for a given time. In summary, the confidence level p determines the droop gain, as shown in Fig. 6.

There may be chattering and oscillation around the switching surface due to the variable structure control. For bounded disturbances and uncertainties, the Lyapunov function should still move toward zero [30]. Thus, convergence analysis can be performed by defining the control law as $\dot{s}(x) \cdot s(x) < 0$. Given a fixed sampling period, the variable $x = 1/P$ can be

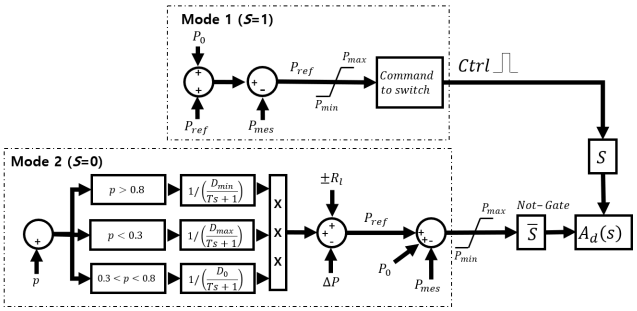

FIGURE 6. Confidence level-based adaptive droop control structure of the ESS.

defined as

$$x = A \cdot D' + B = \frac{D}{P_{delta} - R_l} + P_0 \tag{16}$$

where P_{delta} is the ΔP values integrated for a given sampling time. Thus, P_{delta} and R_l are considered time-invariant values, and the state-space equation can be written as $\dot{x} = A \cdot \dot{D}'$. Considering that D_0 is constant for linearization, the input signal $u$can be written as $T \cdot \dot{D}' + D_0 = u$. Then, u is defined in the control law, and the switching surface $s(x)$ is given by $s(x) = x - t_s/P_{delta}$, and the product of $s(x)$ and its derivative is given by $\dot{s}(x) \cdot s(x) = \dot{x} \cdot s(x) = A/T \cdot (-D_0 + u) \cdot (x)$. Considering the droop gain range, we have $\dot{s}(x) \cdot s(x) < 0$. In conclusion, the proposed adaptive droop control strategy does not degrade the ramp-rate control dynamics further than the fixed droop strategy [31]. The final RMS workflow is illustrated in Fig. 7, and it aligns with the contents of Fig. 1.

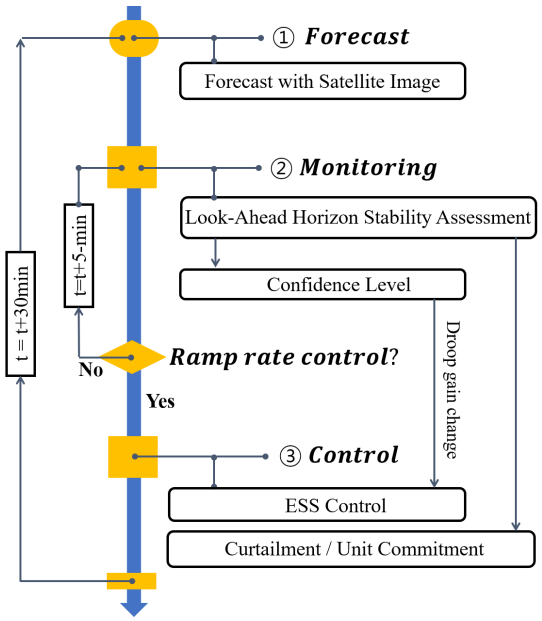

FIGURE 7. Proposed RMS workflow for ESS control.

IV. RESULTS AND DISCUSSION

A. VOLTAGE SOURCE INTERFACE OF THE ESS MODEL

For verification, the proposed control strategy for the Korean RMS model was simulated on the IEEE-39 standard network

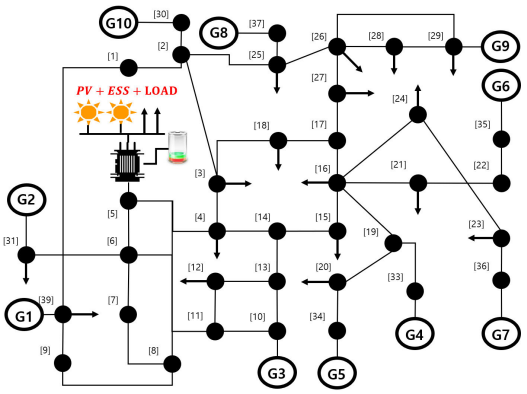

FIGURE 8. Modified IEEE-39 standard bus system.

depicted in Fig. 8, which was modified to add a solar power plant and ESS. SOC_{min} *and* SOC_{max} were set to 0.2 and 0.8, respectively. The total energy of the ESS was assumed as 10 MWh; thus, the discharging time can be calculated as $T = \frac{\left(\frac{6MWh}{10MWh}\right) \times (60 \times 60 \times 1h)}{0.8 - 0.2} = 3{,}600$s. The maximum output power for 1 h was $\frac{8MWh - 2MWh}{1h} = 6MWh$. The maximum current was calculated as $I_{max} = \frac{10MVA}{10MW} = 1$.he calculated parameters were used in the dynamic ESS models REGC_1, REPC_A, and REECC_1. The nominal droop gain D_0, minimum droop gain D_{min}, and maximum droop gain D_{max} were set to 0.035, 0.012, and 0.1, respectively.

To test the effectiveness of the proposed strategy, two cases were considered. As shown in Figs. 9 and 10, the power fluctuation ΔP at bus 5 significantly exceeded the ramp-rate limit of 1.0. Based on the stability assessment results, specific combinations of RES patterns may overload the transmission lines and consume the primary reserve. In the two cases, the objective was to attenuate the power fluctuation via ESS control while optimizing the battery SOC for different levels of confidence in the forecast accuracy. The solar power profiles in Fig. 9 are based on actual measured data from plants. The demand profiles were the same as those used in the test case. To mimic real grid operations, the automatic generation control of conventional generators with area control error was also included in both cases. The area control error can be calculated by $-10 \times B \times (f_{mes} - f_0)$. B and f_0 were set to 0.625 and 50, respectively. Every 5 min, the 30-min-ahead forecast of solar irradiance (total 12-h-ahead a day) and confidence level p were computed. The forecast values were then used to calculate the confidence levels, as shown in Figs. 11 and 12. Because of the lack of historical solar data for the IEEE-39 standard system, both the copula function and confidence level were generated by applying actual measurements from Jeonnam in South Korea.

B. PERFORMANCE EVALUATION

1) CASE 1: HIGH CONFIDENCE LEVEL

In case 1, the standard ramp rate R_s was set to 0.5. The power fluctuation ΔP at bus 5 is represented by a gray line

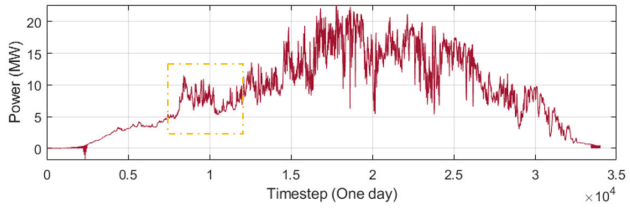

FIGURE 9. Solar power profiles at bus 5.

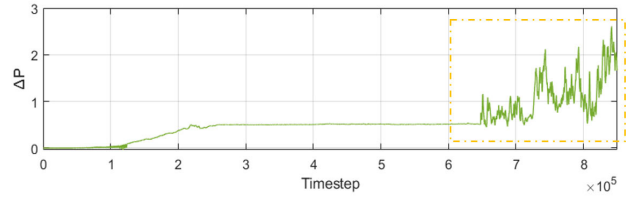

FIGURE 10. Ramp-rate standard violation due to solar profiles.

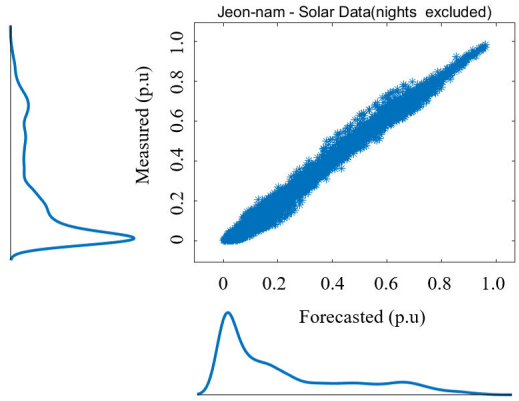

FIGURE 11. Copula function result at Jeonnam.

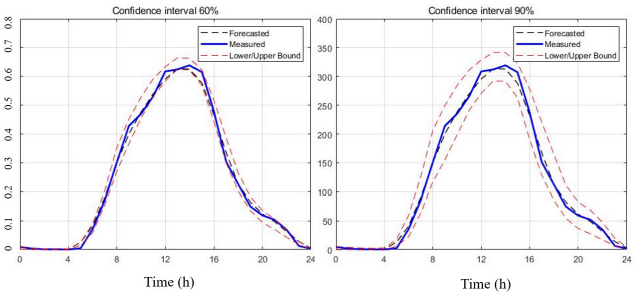

FIGURE 12. Confidence level analysis.

in Fig. 13. The key feature is that variation in the solar power generated variability at bus 5; thus, further charging and discharging of the ESS could not be allowed when the SOC hit its limit. An infeasible starting point was used for the next control process so that the rest of the RESs, which are dispatchable, can be curtailed. The fixed droop gain yielded a fast response but rapidly reached the SOC constraint; this is to be expected because the confidence level was not considered. A value of $p = 0.9$ indicates a larger forecast error than when $p = 0.6$. Thus, a slow response is recommended for better SOC management. After time step 5, a small ΔP occurred at

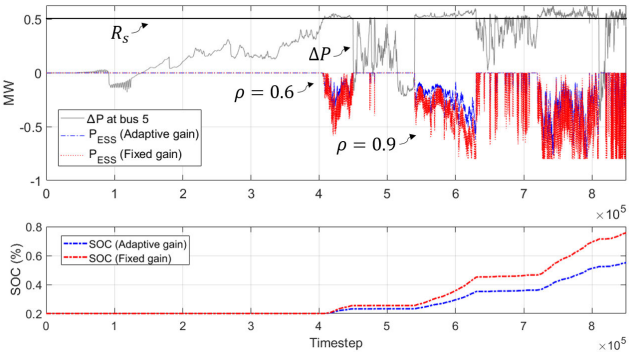

FIGURE 13. ΔP at substation, ESS active power. and SOC in case 1.

the substation, as shown by the gray line, but the ESS rapidly reached SOC_{max} with the fixed droop strategy. However, with the proposed adaptive droop control strategy, the droop gain was changed to D_{min}. Better SOC management was achieved while a slow d-axis current response was injected into the grid. This is because the ESS received confidence level information from the RMS, as depicted in time steps 4–8.5. The proposed strategy allowed for effective SOC management while maintaining a reserve for abrupt changes in solar power.

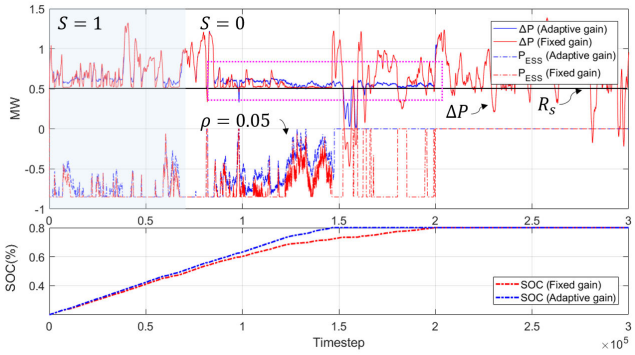

FIGURE 14. ΔP at substation, ESS active power. and SOC in case 2.

2) CASE 2: LOW CONFIDENCE LEVEL

In case 2, the binary signal S was switched to zero because ramp-rate control was introduced after time step 0.75. Then, the confidence level p= 0.05 was transmitted from the RMS, and droop gain was set to D_{max} because a large ΔP with a low forecast error was expected. Thus, a fast response was recommended to suppress variability from the solar power. These actions are depicted by the pink square box in Fig. 14. With the fixed droop gain strategy, ΔP due to changes in solar power greatly exceeded the standard R_s after time step 1.4, as shown by the red line. With the proposed adaptive droop control strategy, ΔP was greatly reduced at bus 5 because a fast d-axis current response was injected into the grid, as shown by the blue line. The volatility of the solar power output was suppressed to the maximum extent, and there were no stability issues during this period. These results demonstrate that the proposed strategy can reduce RES curtailment and help stabilize grid operation. New ESS control strategies

outside the scope of this study can also be integrated with the Korean RMS for further RES penetration.

V. CONCLUSION

This paper presents a comprehensive framework for the Korean RMS and operation of an ESS. The presented framework offers improved forecasting for large-scale grids, real-time stability assessment, the generation of RES penetration scenarios for grid planning, and a novel ESS control strategy to reduce RES curtailment. Simulation results demonstrated that the proposed strategy yields a low-RES curtailment level in grids with high RES penetration and improved ramp-rate control while satisfying operational constraints. Future research will focus on demonstrating the integration of ESSs with the Korean RMS.

REFERENCES

[1] D. Liu, X. Zhang, and C. K. Tse, "Effects of high level of penetration of renewable energy sources on cascading failure of modern power systems," *IEEE J. Emerg. Sel. Topics Circuits Syst.*, vol. 12, no. 1, pp. 98–106, Mar. 2022.

[2] G. Kim, H. Shin, and J. Hur, "Probabilistic estimation of wind generating resources based on the spatio-temporal penetration scenarios for power grid expansions," *IEEE Access*, vol. 9, pp. 15252–15258, 2021, doi: 10.1109/ACCESS.2021.3052513.

[3] S. Song, C. Han, S. Jung, M. Yoon, and G. Jang, "Probabilistic power flow analysis of bulk power system for practical grid planning application," *IEEE Access*, vol. 7, pp. 45494–45503, 2019, doi: 10.1109/ACCESS.2019.2909537.

[4] B. Mohandes, M. Wahbah, M. S. E. Moursi, and T. H. M. El-Fouly, "Renewable energy management system: Optimum design and hourly dispatch," *IEEE Trans. Sustain. Energy*, vol. 12, no. 3, pp. 1615–1628, Jul. 2021, doi: 10.1109/TSTE.2021.3058252.

[5] G. Li, S. Xie, B. Wang, J. Xin, Y. Li, and S. Du, "Photovoltaic power forecasting with a hybrid deep learning approach," *IEEE Access*, vol. 8, pp. 175871–175880, 2020, doi: 10.1109/ACCESS.2020.3025860.

[6] F. Hafiz, M. A. Awal, A. R. D. Queiroz, and I. Husain, "Real-time stochastic optimization of energy storage management using deep learning-based forecasts for residential PV applications," *IEEE Trans. Ind. Appl.*, vol. 56, no. 3, pp. 2216–2226, May 2020, doi: 10.1109/TIA.2020.2968534.

[7] B. V. Solanki, K. Bhattacharya, and C. A. Cañizares, "A sustainable energy management system for isolated microgrids," *IEEE Trans. Sustain. Energy*, vol. 8, no. 4, pp. 1507–1517, Oct. 2017, doi: 10.1109/TSTE.2017.2692754.

[8] F. Yang, X. Feng, and Z. Li, "Advanced microgrid energy management system for future sustainable and resilient power grid," *IEEE Trans. Ind. Appl.*, vol. 55, no. 6, pp. 7251–7260, Nov. 2019, doi: 10.1109/TIA.2019.2912133.

[9] Y. Cui, Y. Wang, Y. Xu, and Y. Zhao, "Low-carbon economic dispatching of microgrid considering generalized integrated demand response and nonlinear conditions," *Energy Rep.*, vol. 9, pp. 1606–1620, Dec. 2023, doi: 10.1016/j.egyr.2022.12.049.

[10] G. Barchi, G. Miori, D. Moser, and S. Papantoniou, "A small-scale prototype for the optimization of PV generation and battery storage through the use of a building energy management system," in *Proc. IEEE Int. Conf. Environ. Elect. Eng., IEEE Ind. Commercial Power Syst. Eur. (EEEIC/I&CPS Europe)*, Jun. 2018, pp. 1–5, doi: 10.1109/EEEIC.2018.8494012.

[11] H. T. Dinh, J. Yun, D. M. Kim, K.-H. Lee, and D. Kim, "A home energy management system with renewable energy and energy storage utilizing main grid and electricity selling," *IEEE Access*, vol. 8, pp. 49436–49450, 2020, doi: 10.1109/ACCESS.2020.2979189.

[12] R. Kandari, P. Gupta, and A. Kumar, "Battery state of charge based improved adaptive droop control for power management of a microgrid having large scale renewable generation," *Sustain. Energy Technol. Assessments*, vol. 57, Jun. 2023, Art. no. 103146, doi: 10.1016/j.seta.2023.103146.

[13] K. Bi, W. Yang, D. Xu, and W. Yan, "Dynamic SOC balance strategy for modular energy storage system based on adaptive droop control," *IEEE Access*, vol. 8, pp. 41418–41431, 2020, doi: 10.1109/ACCESS.2020.2976729.

[14] Z. Ren, W. Yan, X. Zhao, W. Li, and J. Yu, "Chronological probability model of photovoltaic generation," *IEEE Trans. Power Syst.*, vol. 29, no. 3, pp. 1077–1088, May 2014, doi: 10.1109/TPWRS.2013.2293173.

[15] M. Kang, R. Zhu, D. Chen, C. Li, W. Gu, X. Qian, and W. Yu, "A cross-modal generative adversarial network for scenarios generation of renewable energy," *IEEE Trans. Power Syst.*, 2023, doi: 10.1109/TPWRS.2023.3277698.

[16] D. N. Walters et al., "The met office unified model global atmosphere 4.0 and JULES global land 4.0 configurations," *Geosci. Model Develop.*, vol. 7, no. 1, pp. 361–386, 2014, doi: 10.5194/gmd-7-361-2014.

[17] F. A. Eckel and L. D. Monache, "A hybrid NWP–Analog ensemble," *Monthly Weather Rev.*, vol. 144, no. 3, pp. 897–911, Mar. 2016, doi: 10.1175/mwr-d-15-0096.1.

[18] S. Hemri and B. Klein, "Analog-based postprocessing of navigation-related hydrological ensemble forecasts," *Water Resour. Res.*, vol. 53, no. 11, pp. 9059–9077, Nov. 2017, doi: 10.1002/2017wr020684.

[19] C. K. Kim, H.-G. Kim, Y.-H. Kang, C.-Y. Yun, B. Kim, and J. Y. Kim, "Solar resource potentials and annual capacity factor based on the Korean solar irradiance datasets derived by the satellite imagery from 1996 to 2019," *Remote Sens.*, vol. 13, no. 17, p. 3422, Aug. 2021, doi: 10.3390/rs13173422.

[20] A. Iravani and F. de León, "Real-time transient stability assessment using dynamic equivalents and nonlinear observers," *IEEE Trans. Power Syst.*, vol. 35, no. 4, pp. 2981–2992, Jul. 2020, doi: 10.1109/TPWRS.2020.2968293.

[21] S. Jafarzadeh and V. M. I. Genc, "Real-time transient stability prediction of power systems based on the energy of signals obtained from PMUs," *Electr. Power Syst. Res.*, vol. 192, Mar. 2021, Art. no. 107005, doi: 10.1016/j.epsr.2020.107005.

[22] A. Safavizadeh, M. Kordi, F. Eghtedarnia, R. Torkzadeh, and H. Marzooghi, "Framework for real-time short-term stability assessment of power systems using PMU measurements," *IET Gener., Transmiss. Distrib.*, vol. 13, no. 15, pp. 3433–3442, Aug. 2019.

[23] A. Safavizadeh, M. Kordi, F. Eghtedarnia, R. Torkzadeh, and H. Marzooghi, "Framework for real-time short-term stability assessment of power systems using PMU measurements," *IET Gener., Transmiss. Distrib.*, vol. 13, no. 15, pp. 3433–3442, Aug. 2019, doi: 10.1049/iet-gtd.2018.5579.

[24] G. Papaefthymiou and D. Kurowicka, "Using copulas for modeling stochastic dependence in power system uncertainty analysis," *IEEE Trans. Power Syst.*, vol. 24, no. 1, pp. 40–49, Feb. 2009, doi: 10.1109/tpwrs.2008.2004728.

[25] M. Sklar, "Fonctions de répartition à n dimensions et leurs marges," *Annales de l'ISUP*, vol. 8, no. 3, pp. 229–231, 1959.

[26] E. Parzen, "On estimation of a probability density function and mode," *Ann. Math. Statist.*, vol. 33, no. 3, pp. 1065–1076, Sep. 1962, doi: 10.1214/aoms/1177704472.

[27] *Model-Free Renewables Scenario Generation Using Generative Adversarial Networks*. Accessed: Nov. 30, 2023. [Online]. Available: https://github.com/chennnnnyize/Renewables_Scenario_Gen_GAN

[28] F. Calero, C. A. Cañizares, K. Bhattacharya, C. Anierobi, I. Calero, M. F. Z. de Souza, M. Farrokhabadi, N. S. Guzman, W. Mendieta, D. Peralta, B. V. Solanki, N. Padmanabhan, and W. Violante, "A review of modeling and applications of energy storage systems in power grids," *Proc. IEEE*, vol. 111, no. 7, pp. 806–831, Jul. 2022.

[29] B. Zhang, F. Gao, Y. Zhang, D. Liu, and H. Tang, "An AC-DC coupled droop control strategy for VSC-based DC microgrids," *IEEE Trans. Power Electron.*, vol. 37, no. 6, pp. 6568–6584, Jun. 2022, doi: 10.1109/TPEL.2022.3141096.

[30] S. Song, R. A. McCann, and G. Jang, "Cost-based adaptive droop control strategy for VSC-MTDC system," *IEEE Trans. Power Syst.*, vol. 36, no. 1, pp. 659–669, Jan. 2021, doi: 10.1109/TPWRS.2020.3003589.

[31] J. Marcos, O. Storkël, L. Marroyo, M. Garcia, and E. Lorenzo, "Storage requirements for PV power ramp-rate control," *Sol. Energy*, vol. 99, pp. 28–35, Jan. 2014, doi: 10.1016/j.solener.2013.10.037.

[32] J. Martins, S. Spataru, D. Sera, D.-I. Stroe, and A. Lashab, "Comparative study of ramp-rate control algorithms for PV with energy storage systems," *Energies*, vol. 12, no. 7, p. 1342, Apr. 2019, doi: 10.3390/en12071342.

[33] J. M. Guerrero, M. Chandorkar, T.-L. Lee, and P. C. Loh, "Advanced control architectures for intelligent microgrids—Part I: Decentralized and hierarchical control," *IEEE Trans. Ind. Electron.*, vol. 60, no. 4, pp. 1254–1262, Apr. 2013, doi: 10.1109/TIE.2012.2194969.
[34] X. Su, X. Liu, P. Shi, and R. Yang, "Sliding mode control of discrete-time switched systems with repeated scalar nonlinearities," *IEEE Trans. Autom. Control*, vol. 62, no. 9, pp. 4604–4610, Sep. 2017, doi: 10.1109/TAC.2016.2626398.

SUNGYOON SONG (Member, IEEE) received the B.S. degree in electrical engineering from Soongsil University, Seoul, South Korea, in 2015, and the M.S. and Ph.D. degrees in electrical engineering from Korea University, Seoul, in 2020. From 2020 to 2021, he was a Senior Researcher with the Korea Institute of Energy Research (KIER), Daejeon, South Korea. He is currently a Senior Researcher with the Korea Electrotechnology Research Institute (KERI), Uiwang-si, South Korea. His research interests include modeling and control of HVdc/FACTS, and energy management systems (EMS) with AI applications.

SUNGWOO KANG (Graduate Student Member, IEEE) received the B.S. degree in energy systems engineering from Chung-Ang University, Seoul, South Korea, in 2019. He is currently pursuing the joint M.S. and Ph.D. degree with Korea University, Seoul. His research interests include the integration of renewable energy sources and the impact analysis of renewable energy sources on power system stability and operation.

SANGHO LEE (Member, IEEE) received the B.S., M.S., and Ph.D. degrees in electrical engineering from Seoul National University, South Korea, in 1995, 1997, and 2003, respectively. He is currently the Executive Director of the Korea Electrotechnology Research Institute. His research interests include EMS application and power system stability.

CHANG KI KIM (Member, IEEE) received the B.S., M.S., and Ph.D. degrees in atmospheric sciences from Yonsei University, Seoul, South Korea, in 2003, 2006, and 2011, respectively. He is currently a Distinguished Principal Researcher with the Renewable Energy Big Data Laboratory, Korea Institute of Energy Research. With a career spanning diverse geographical locations, including postdoctoral roles in the USA, he has amassed extensive expertise in numerical modeling of the atmospheric boundary layer, cloud dynamics, and interactions involving aerosols, clouds, and ice crystals. His research interests include solar irradiance forecasting and blending numerical modeling with satellite imagery to advance the field of renewable energy.